Accelerated clearing and molecular labeling of biological tissues using magnetohydrodynamic force

Joseph Dwyer
University of Massachusetts Amherst
M. Desmond Ramirez
University of Massachusetts Amherst
Paul S. Katz
University of Massachusetts Amherst
Rolf O. Karlstrom
University of Massachusetts Amherst
Joseph F. Bergan (jbergan@umass.edu)
University of Massachusetts Amherst

Research Article

Keywords: fluorescence microscopy, magnetohydrodynamic force

Posted Date: February 26th, 2021

DOI: https://doi.org/10.21203/rs.3.rs-213122/v1

Version of Record: A version of this preprint was published at Scientific Reports on August 12th, 2021.
See the published version at https://doi.org/10.1038/s41598-021-95692-2.

Abstract

Techniques used to clear biological tissue for fluorescence microscopy are essential to connect anatomical principles at levels ranging from subcellular to the whole animal. Here we report a simple and straightforward approach to efficiently render opaque tissue samples transparent and show that this approach can be modified to rapidly label intact tissue samples with antibodies for large volume fluorescence microscopy. This strategy applies a magnetohydrodynamic (MHD) force to accelerate the removal of lipids from tissue samples at least as large as an intact adult mouse brain. We also show that MHD force can be used to accelerate antibody penetration into tissue samples. This strategy complements a growing array of tools that enable high-resolution 3-dimensional anatomical analyses in intact tissues using fluorescence microscopy. MHD-accelerated clearing is simple, fast, reliable, inexpensive, provides thermal regulation, and is compatible with existing strategies for high-quality fluorescence microscopy of intact tissues.

Introduction

Advances in microscopy now allow investigation of subcellular anatomical structures while maintaining the macroscopic organization of intact tissues. Generating high-quality tissue samples is a critically important step towards achieving this goal. Most biological tissues, including the brain, are recalcitrant to large-volume microscopy without first being made optically transparent (cleared). Early methods for chemically-based tissue clearing quenched fluorescence, making tissue samples unsuitable for fluorescence microscopy (Shultze, et al., 1897; Spalteholz, et al., 1914); however, modern approaches for tissue preparation reduce light scattering without quenching fluorescence (Chung, et al., 2013; Hama, et al., 2011; Kim, et al., 2015; Renier, et al., 2016; Li, et al., 2018; Susaki, et al., 2020; Supplementary Table 1). These approaches reduce light scattering primarily by removing lipids and standardizing the refractive index of the tissue sample. When combined with genetically encoded fluorophores, these approaches enable anatomical investigation with sub-micron precision at depths of at least a centimeter. Here, we present a technique that utilizes MHD force in combination with a conductive buffer and detergent to prepare high-quality cleared tissue samples efficiently, reliably, and cost-effectively for visualization with fluorescence microscopy. Importantly, MHD-based clearing minimizes thermal damage to tissue, preserves endogenous fluorescent signals, and is simple to implement.

MHD force describes a physical phenomenon also known as Lorentz force where force is generated on a charged particle in the third orthogonal direction from perpendicular electric and magnetic fields (Jamalabadi, 2014). The efficiency of MHD force to rapidly drive charged molecules into and out of tissue is a consequence of a fundamental difference in the way that MHD fields and electrical fields act on charged particles. Electrophoresis drives cations and anions in opposite directions resulting in no net flow of buffer through a tissue sample. In contrast, MHD-forces drive cations and anions in the same direction along the third orthogonal axis resulting in a unidirectional flow of buffer through the sample itself (Fig. 1C; Jamalabadi, 2014). The rapid flow of buffer through a tissue sample located within the MHD field (Video 1) constantly replaces heated buffer with fresh cool buffer thereby minimizing thermal

damage to fluorescent molecules embedded in a large tissue sample while rapidly removing unbound molecules.

Intact tissues also present a challenge for the introduction of molecules that are needed to label molecular features deep in the sample. Based on the efficacy of MHD-accelerated clearing, we tested if MHD force could be used to propel antibodies into tissue samples. The same approach used to remove lipids and clear tissue samples also accelerated the penetration of antibodies into the tissue sample—MHD-accelerated labeling.

Using MHD-accelerated clearing, transparency of an intact mouse brain can be achieved in as little as 12 hours. MHD forces can subsequently be harnessed to drive antibodies into cleared tissues. These MHD-based approaches work in both vertebrate (shown for mouse and zebrafish) and invertebrate (shown for the nudibranch mollusk *Berghia stephanieae*) species, providing a generalizable method to render intact tissue transparent and accelerate immunohistochemical labeling for fluorescence microscopy of intact tissues. We provide plans for the construction of the MHD device, as well as a detailed protocol to ensure the successful implementation of this strategy for those interested in large-volume tissue microscopy.

Results

Effects of MHD force

MHD force produces a linear increase in flow velocity that is not observed with the application of purely electrical force (Fig. 1). To quantify the effects of the MHD force, we compared the movement of sodium alginate spheres suspended in an electrically conductive buffer in response to purely electrical or MHD forces. The MHD condition produced dramatically higher velocity flow over the electrical only condition for all tested non-zero voltages and across the time course (Fig. 1A; $p < 0.0001$). The difference between MHD and electric-only flow velocity increased as the applied voltage increased (Fig. 1A).

Tissue Clearing/Delipidation

MHD-accelerated clearing renders an intact mouse brain transparent in as little as 12 hours (Fig. 2). Both electric-only and MHD-accelerated clearing remove lipids from brain tissue and produce an increasingly transparent tissue sample with longer clearing times (Fig. 2B). Tissue samples cleared using MHD-accelerated clearing were cleared more completely and quickly than electric-only clearing (30V DC; 0.35 AMPS). As the electric-only condition does not produce buffer flow independently, these trials were conducted with the assistance of a peristaltic pump (500 ml/min) with flow matched to the MHD condition to prevent tissue damage from overheating.

Because excessive heating during active clearing can denature proteins and quench fluorescence, we measured the temperature of tissue samples actively cleared with either MHD or electric-only conditions at matched voltage, amperage, and buffer circulation (Fig. 2C). Note that the buffer circulation for the MHD condition is intrinsic to the technique while a pump is required to achieve buffer flow with the

electric-only condition. The temperature of brains cleared in the electric-only condition were hotter temperatures than those cleared in the MHD condition across the full range of tested voltages indicating that MHD-accelerated clearing provides additional thermal buffering ($F(1,3) = 119$, $p < 0.0001$; 2-way anova with repeated measures).

MHD-accelerated clearing reliably rendered tissue samples optically transparent while also preserving genetically encoded fluorescent proteins (Fig. 3). An intact adult mouse brain conditionally expressing GFP via EnvA-G-deleted rabies virus in aromatase-expressing neurons (Watabe-Uchida et al., 2016; Yao, et al., 2017; Billing et al., 2020) was prepared using MHD-accelerated clearing. Without fluorescent labeling, the shadows of individual cells and fine subcortical architecture (e.g., anterior commissure) is visible into the very center of the tissue (Fig. 3A). A population of GFP-expressing cells was easily identified in the medial amygdala (Fig. 3A). Higher magnification images showed that fine processes, such as dendrites and axons, can be identified and analyzed several millimeters (3 mm) from the surface of the brain (Fig. 3B; Video 2). Indeed, the resolution is sufficient to reconstruct the dendritic arbors of individual neurons in three dimensions (Fig. 3C; Fig. 3D) and to reconstruct the path of a single axon, including axon collaterals, from the cell body, through several millimeters of brain tissue, ending at the axon terminals (Fig. 3E).

Tissue Labeling: MHD-accelerated labeling improved antibody penetration and allowed labeling of large intact tissue samples (Fig. S1). To confirm the specificity of antibody binding is maintained in MHD-accelerated labeling, we used an anti-vasopressin antibody in mice that expressed tdTomato in vasopressin-expressing neurons (Fig. 4A-C). Tissue was generated by crossing the Ai9 Rosa26:LSL:tdTomato reporter line (Madisen, et al., 2010) and a line where Cre recombinase is expressed under the control of the arginine vasopressin (AVP) promoter (Bendesky, et al., 2017). This produced tissue where the fluorescent reporter tdTomato was expressed under the control of the AVP promoter. After a 12-hour MHD accelerated antibody label on this tissue using an anti-AVP antibody, we observed specific co-labeling of the genetically encoded fluorophores and the anti-AVP antibody (Fig. 4A-C).

An intact adult nudibranch (*Berghia stephanieae*) (medio-lateral: 1.3 mm, dorso-ventral: 1.5 mm, anterio-posterior: 2 cm) that had been delipidated using the MHD-accelerated clearing device was incubated with an anti-serotonin (5-HT; Immunostar; 1:500) antiserum followed by a fluorescent secondary antibody (488 nm conjugated; ThermoFisher; 1:200) suspended in a high pH electrophoresis buffer (0.1 M Borate Buffer and 0.1% Triton X-100 brought to pH 9.5 with 0.1 M LiOH; Fig. S2). Passive incubation for 12 hours resulted in little to no penetration into the brain (Fig. 4D), whereas MHD-accelerated antibody labeling for 12 hours drove antibodies throughout the sample and revealed 5-HT expressing cell bodies and neurites (Fig. 4E).

Intact zebrafish brains (medio-lateral: 3 mm; dorso-ventral: 3 mm; anterio-posterior: 6 mm) were passively delipidated in SDS for 7 days and then incubated with anti-acetylated tubulin antiserum (Immunostar; 1:500; Piperno, et al., 1985) for 12 hours to identify neural fibers (Fig. 4G). Control tissue samples (no MHD force applied) showed minimal antibody penetration along the outer edge of the tissue with little

fluorescence visible in the optic tectum (Fig. 4F). In contrast, MHD-accelerated labeling for the same amount of time showed robust labeling of neural tracts throughout the brain (Fig. 4G).

To test MHD-accelerated labeling in mammalian tissue, an anti-oxytocin (OT) antibody was applied to a cube of mouse brain (medio-lateral: 6 mm, ventro-dorsal: 6 mm, antero-posterior: 6 mm) centered on the periventricular nucleus of the hypothalamus (1:500 primary; 1:200 secondary). As above, antibodies did not effectively penetrate the tissue sample in the absence of MHD force (Fig. 4H). In contrast, OT-expressing cells were clearly visible in the PVN, located deep within of tissue cube, using MHD-accelerated labeling (Fig. 4I). OT-expressing neuronal processes were easily resolved and were seen to project towards the third ventricle, which is consistent with OT neuron morphology (Fig. S2). Accurate OT-labeling was seen > 1.8 mm from the nearest edge. The ability to visualize axonal varicosities and nuclei in OT-labeled neurons demonstrated that the MHD-accelerated labeling strategy can be used to resolve subcellular structures (Fig. 4I).

Discussion

The ability to study fine anatomical structures while maintaining their native organization is necessary to reveal relationships at the wide range of scales over which biological functions occur. The MHD-accelerated protocol outlined here harnesses the strengths of hydrogel-based clearing approaches to maintain proteins and genetically encoded fluorescence in large samples (Chung, et al., 2013; Kim, et al., 2015; Susaki, et al., 2015; Lee, et al., 2016; Pan, et al., 2016). MHD accelerated clearing maintains all advantages of electric-only clearing and adds the additional MHD force to further accelerate tissue clearing without increasing the potentially damaging electric field (Fig. 2; Fig. 4—Fig. S1).

MHD-induced flow serves at least three purposes. First, in the case of tissue clearing it helps remove lipids from the tissue sample. Second, in the case of antibody labeling it helps push antibodies into the tissue. While MHD acts directly on electrically charged antibodies, it is also possible that the observed acceleration of antibody penetration is because MHD generates something akin to a stream of buffer flowing inside the fixed tissue. Like twigs caught in the flow of a river, antibodies and lipids could be pulled through the tissue sample allowing rapid clearing and labeling. Third, MHD driven buffer flow provides additional thermal regulation of tissue samples above that observed with electrophoretic-only approaches (Fig. 1). The MHD force is produced within the tissue itself and therefore constantly pulls fresh cool buffer into the tissue sample to replace buffer that has been heated by the electrical resistance (Fig. 1). Because buffer flow is inherent to the MHD process, no moving parts (e.g. pump) are required to maintain buffer flow and the resultant thermal buffering. Moreover, because the ‘pumping’ action of MHD is produced directly from the electrical and magnetic fields, tissue damage resulting from pump failure during active clearing is almost completely eliminated with MHD-accelerated tissue clearing.

This approach does not rely on solvents that are harmful to fluorophores (e.g., methanol and hydrogen peroxide), and simplifies tissue clearing to the bare minimum components. The only obligatory requirement is that the tissue sample is held at the intersection of an electrical and a magnetic field.

Thus, the strategy outlined here is clean, efficient, and adaptable. The device itself can be 3D printed in plastic (Fig. 5; Supplementary Files) making the device simple and cost-effective, roughly two-hundred dollars, to build.

The MHD-based approach described here (Fig. 5; Fig. 6) reliably allows rapid tissue clearing, rendering them suitable for three-dimensional fluorescent imaging. We demonstrate the efficacy of a simple MHD device by clearing dozens of mouse brains and measuring the effects of voltage and MHD-conjugation on tissue heat, clarity and time needed to achieve complete optical transparency. We also introduce the exciting possibility by labeling sea slug, zebrafish, and mouse tissue with multiple different antibodies. Each antibody protocol required no more than 4.5 mL (1:200 concentration) of labeling solution which can be collected at the end of the procedure and reused. Similarly, the buffer solution used for clearing can be reused until the pH falls below 8.2 (typically after one month of heavy use or about 20 brains). Taken together, we believe MHD-accelerated clearing and labeling provides a simple, reliable, effective, and economical approach that can also be quickly adapted to the specific needs of each experiment.

Methods

All the protocols adhered to the ARRIVE guidelines with the limited exception that antibody staining and clearing effectiveness was measured unblind. In these instances of unblinded data collection, the data analysis was conducted blind.

Animal Use

All use of vertebrate animals including animal care and experimentation was carried out in accordance with NIH and ARRIVE guidelines.
All procedures involving animals were approved by the Institutional Animal Care and Use Committee at the University of Massachusetts in Amherst (IACUC; protocol #2018-0014 and #2017-0060) and conducted in accordance with protocols approved by IACUC and in adherence with all relevant regulations and directives on animal care.
Euthanasia of mice was performed using isoflurane (2–5%) to induce deep anesthesia followed by cervical dislocation.

Measure of MHD-induced flow

A solution of sodium chloride was made in a small tank (2.5 L). Sodium chloride was slowly added to the tank until the electric conductivity of the solution matched that of the clearing solution. The clearing device was then submerged in the solution with a measured grid behind the tank to provide scale. 0V, 10V, 20V, 30V, 40V, 50V, or 60V were applied to the device and sodium alginate spheres were introduced into the tank at a constant location (N = 7). The velocity of the spheres through the device was measured. Velocity was calculated using a high-speed video taken over a calibrated grid. This process was then repeated using only an electric field (magnets were removed). Paired-sample t-tests were performed between the MHD and electric-only conditions at each voltage and a 2-way ANOVA was performed across

all voltages using MATLAB. The p-values for the paired samples T-test were corrected for multiple comparisons using Bonferroni correction. Each condition was fit to a linear model using MATLAB.

Design of MHD-accelerated clearing device

The strategy for using MHD to remove lipids from tissue samples requires binding proteins and polymerizing a hydrogel, removing lipids, and matching the refractive index of the tissue and imaging media (Fig. 5A). A tissue chamber was placed into the central chamber of the MHD-accelerated clearing device (Fig. 5B, C). This holds the tissue at the intersection of the electrical and magnetic fields. The clearing chamber was submerged in a large (5 L) bath of clearing solution at 37°C and 30 VDC (0.35 Amps) was applied across the tissue for several hours (typically 16 hours for mouse brain tissue and 2 hours for intact zebrafish brains; Fig. 5D).

Tissue Fixation and hydrogel polymerization

Mice were anesthetized with isoflurane, euthanized, and perfused with 0.01 M phosphate buffered saline (PBS) followed by 4% paraformaldehyde (PFA) in 0.01M PBS.
Tissue was then post-fixed in 4% PFA at 4 ˚C overnight. Next, the tissue was placed in a hydrogel solution (4% acrylamide, 4% PFA, 0.05% bis acrylamide, and 0.25% VA-044 initiator suspended in 0.01 M PBS) at 4 ˚C overnight (Chung, et al., 2013; Isogai, et al., 2017). Oxygen was flushed out of hydrogel-infused tissues nitrogen gas and then the samples were polymerized by incubating them at 37 ˚C overnight (Chung, et al., 2013). Excess hydrogel was removed from the surface and tissue samples were transferred to PBS to flush hydrogel monomers.

Adult zebrafish were euthanized in 0.2 mg/ml tricaine mesylate (MS-222), decapitated, and the heads placed in 4% paraformaldehyde overnight. Heads were then placed in PBS and brains were carefully dissected, incubated in hydrogel at 4 ˚C overnight, and processed as above.

Adult nudibranchs (*Berghia stephanieae*) were anaesthetized in cold 4.5% magnesium chloride in artificial sea water for 20 minutes, pinned to a Sylgard-lined dish, and fixed in 4% paraformaldehyde in sea water overnight at 4 ˚C. Whole animals were washed with PBS and then incubated in hydrogel at 4 ˚C overnight and processed as above.

Active Tissue Delipidation (clearing): Tissue samples were incubated in SDS-clearing solution (10 mM sodium dodecyl sulfate in 0.1 M borate buffer, pH 8.5) for 2 days at 37 ˚C unless otherwise noted. Samples were then transferred to the MHD-accelerated clearing chamber, consisting of two interlocking cell-strainers (ThermoFisher; catalog #: 87791). This chamber was placed in the intersection of the electrical and magnetic fields in the center of the device and the chamber was lowered into a bath of 37 ˚C SDS. 30V DC were then applied across the tissue to initiate MHD-accelerated clearing (Fig. 5D). After clearing, the tissue is taken out of the clearing chamber and washed in 0.1 M PBS for at least 12 hours. Of the 55 samples cleared for this paper using this technique in multiple laboratories, all achieved transparency with little physical damage.

Electrophorectic Clearing: Tissue samples were incubated in SDS-clearing solution for 2 days at 37 ˚C unless otherwise noted. Samples were then transferred to a clearing chamber, consisting of two interlocking cell-strainers (ThermoFisher; catalog #: 87791). This chamber was placed between two electrodes in the center of a MHD-accelerated clearing device, which has had magnets removed from the device. A 500ml/min peristaltic pump (Grey Beard Niagra) was then affixed to the top of the central chamber to circulate buffer across the tissue during clearing by pulling buffer from the temperature-controlled bath. The chamber and output from the pump were lowered into a bath of 37 ˚C SDS. Direct electrical current was then applied across the tissue to initiate clearing. After clearing, the tissue was taken out of the clearing chamber and washed in 0.1 M PBS for at least 12 hours.

Clearing Temperature Measurements: Tissue was left to incubate in SDS-clearing solution for 2 days at 37 ˚C, then allowed to cool to room temperature for at least 2 hours. Tissue was then subjected to either MHD-accelerated or electrophoretic clearing (n = 6) for 30 minutes with four different voltages applied across the tissue (30, 40, 50, and 60 VDC) in a 37 ˚C SDS bath. After clearing the tissue was rapidly removed from the device and imaged with an infrared thermal imaging camera (Hti-Xintai: HT-18) on a room temperature background. The highest observed temperature from each sample was recorded and the tissue was allowed to cool down to room temperature prior to additional experiments at different voltages.

Refractive Index Matching and Light Sheet Microscopy

The tissue was transferred to “Optiview” (Isogai, et al., 2017) refractive index matching solution and incubated at 37 ˚C for at least 12 hours to achieve optical clarity through RI matching (Fig. 5A; Isogai, et al., 2017). Samples were imaged at 5X or 20X magnification with a lightsheet microscope adapted for a 1.45 RI imaging solution (Zeiss Z1).

Measures of Clearing Efficacy

Tissue was left to incubate in SDS-clearing solution for 2 days at 37 ˚C. Tissue was then subjected to either MHD-accelerated or electrophoretic clearing (n = 6) for 24 hrs. Clearing was interrupted at 0hr, 6hr, 12hr, and 24hr. Tissue was washed with 0.01M PBS overnight, then equilibrated to RI 1.43 in Optiview (Isogai, et al., 2017) for at least two days at 37 ˚C. Tissue transparency was then measured by the percentage of light transmitted through the tissue suspended in an Optiview solution (Isogai, et al., 2017). Light transmission was measured using a wide-spectrum light-source and calibrated photodiode. The sample was then washed in 0.01M PBS overnight, then equilibrated to SDS-clearing solution for 2 days at 37 ˚C before clearing continued up to 24hr per sample. Data across all samples at each time were fit with a saturating exponential curve in MATLAB.

MHD-accelerated staining of fixed tissue with methylene blue

Penetration of methylene blue into a 1 cm^3 cube of homogeneous brain tissue under MHD force was tested over 1, 2, and 4 hours (N = 1). Cubes of uncleared sheep brain tissue were equilibrated to the

antibody labeling buffer solution for 12 hours. The tissue was then placed at the intersection of a strong magnetic and electric field (30V DC) and submerged in a solution of methylene blue (0.1 M) buffered to pH 9.5 (37°C). The orientation of the electric field was reversed at 15-minute intervals for 3 minutes. Three samples were labeled using this approach for 1, 2 or 4 hours. Following the stain, the tissue was bisected and imaged. A control sample was incubated in the same solution (37°C) for 4 hours without the application of any active force. This sample was bisected and imaged as the others.

Comparative staining of methylene blue into agarose cubes as a result of various strengths of electrical force conjugated to MHD force

15 1 cm^3 of 3 % agarose were subjected to labeling methylene blue labeling by MHD force for 0, 5, 10, 15, 30, 60, or 120 minutes at varied electrical field strengths. The distance penetrated into the agarose cubes was measure after bisection and plotted against staining time with 10, 20, or 30V in a constant magnetic field.

Antibody Labeling: Delipidated tissue was placed inside of a 2-inch length of 0.25-inch diameter dialysis tubing (6–8 kDa); Spectrum). After equilibration, samples were incubated in an antibody solution inside dialysis tubing at the center of intersecting electrical and magnetic fields where the MHD force was strongest (Fig. 6). Confining the tissue sample inside dialysis tubing reduced the volume of antibody required for labeling and protected the tissue sample and antibody solution from direct exposure to the electrodes. Magnets (Applied magnets; NB057-6-N52) were placed on the top and bottom of the MHD labeling device creating a central chamber Fig. 6B). The ends of the dialysis tubing were connected to 9.5 mm diameter vinyl tubing (ThermoFisher: S504591) using 0.25-inch Leur lock barbs (Cole-Parmer; UX-45501-20) to create a torus-shaped chamber allowing the antibody solution to circulate continuously and provide an even and continuous source of antibody to the tissue sample (Fig. 6). Antibody solution (4.5 mL; 0.1 M borate buffer titrated to pH 9.5 with 0.1 M LiOH, 1% heparin, 0.1% Triton X-100; 1:500 primary antibody) was transferred into the dialysis tubing using a 5 mL syringe. The labeling chamber was submerged in a 1L tub containing electrophoresis solution (0.1M Borate Buffer pH 9.5/0.1% Triton X-100 solution). A 5 mL syringe filled with the buffer solution was attached to the circulation line to maintain constant pressure inside of the dialysis tube. 60 volts DC (~ 0.2 Amps) was applied across the electrodes for 15 minutes, followed by 3 minutes of inactivity repeatedly for 12 hours to drive antibodies into the tissue sample. The system was held at 37 ˚C and protected from ambient light to minimize bleaching of fluorophores throughout the procedure.

Following each round of MHD-accelerated labeling, the antibody solution was replaced with a wash solution (0.1 M borate buffer titrated to pH 9.5 with 0.1 M LiOH, 1% heparin, 0.1% Triton X-100) and the tissue was exposed to 6-hours of “active washing” using the same voltage settings. Labeled tissue was then washed in 0.01 M PBS for at least 12 hours.

Traditional Immunohistochemistry: Mouse brains were dissected from highly anesthetized mice. These tissues were incubated in 4% PFA suspended in 0.01M PBS at 4°C. Tissue was sliced to 100 µm

thickness on a vibratome and transferred to 0.01M PBS or the electrophoresis buffer used in MHD-accelerated labeling. Slices were blocked in 10% FBS in 0.5% TritonX-100/PBS or electrophoresis buffer at room temperature for 1 hour, then incubated in a 1:200 dilution of antibody in 10% FBS/PBS or electrophoresis buffer at room temperature for 2 hours. The tissue was then washed three times in 0.05% TritonX-100 / PBS or electrophoresis buffer for 30 minutes at room temperature.

Declarations

Acknowledgements:

We thank D.K., P.S., and the members of the Bergan lab for helpful comments on this paper. Support for these experiments came from the University of Massachusetts at Amherst, the Armstrong Fund for Science (J.F.B), BRAIN U01-NS108637 (P.S.K.), and a generous gift from Britton Sanderford (J.F.B). J.F.D is a recipient of the University of Massachusetts at Amherst NSB Fellowship. This material is based upon work supported by the NSF Postdoctoral Research Fellowship in Biology to M.D.R. under Grant No. (1812017).

Additional Information:

Author contributions: J.F.D. and J.F.B. conceived and designed all experiments. J.F.D. and M.D.R. collected the data. J.F.D. and J.F.B. analyzed the data and wrote the manuscript. P.S.K. and R.O.K. provided reagents and extensive input at all stages of manuscript preparation.

Competing Interests:

A patent application has been submitted by J.F. Bergan and J.F. Dwyer based on this work: UOMA-057US. M.D. Ramirez, P.S. Katz, and R.O. Karlstrom have no competing interests to report.

Data Availability:

All primary data is available upon request to the corresponding author.

References

1. Bendesky, A. *et al.* The genetic basis of parental care evolution in monogamous mice. *Nature.***544** (7651), 434–439 (2017).
2. Billing, A., Correia, M., Kelly, D., Li, G. & Bergan, J. (2020). Synaptic Connections of Aromatase Circuits in the Medial Amygdala Are Sex Specific. eNeuro, 7(3), 0489-19.2020. DOI: https://doi.org/10.1523/ENEURO.0489-19.2020
3. Chi, J., Crane, A., Wu, Z. & Cohen, P. Adipo-Clear: A Tissue Clearing Method for Three-Dimensional Imaging of Adipose Tissue. *Journal of Visualized Experiments.* (137), https://doi.org/10.3791/58271 (2018).

4. Chung, K. *et al.* Structural and molecular interrogation of intact biological systems. *Nature.***497** (7449), 332–337 https://doi.org/10.1038/nature12107 (2013).
5. Hama, H. *et al.* (2011). Scale: a chemical approach for fluorescence imaging and reconstruction of transparent mouse brain.Nature Neuroscience, (14):1481–1488.
6. Hama, H. *et al.* Hioki, Hiroyuki, Namiki, Kana, Hoshida, Tetsushi, Kurokawa, Hiroshi, (2015). ScaleS: an optical clearing palette for biological imaging. Nat Neurosci, 18(10): 1518–1529.
7. Isogai, Y., Richardson, D. S., Dulac, C. & Bergan, J. (2017) Optimized Protocol for Imaging Cleared Neural Tissues Using Light Microscopy. In: Poulopoulos A. (eds) Synapse Development. Methods in Molecular Biology, vol 1538.Humana Press, New York, NY
8. Jamalabadi, M. Y. Analytical Study of Magnetohydrodynamic Propulsion Stability. *J. Marine Sci. Appl.***13**, 281–290 (2014).
9. Kim, S. Y. *et al.* Stochastic electrotransport selectively enhances the transport of highly electromobile molecules. *PNAS.***112** (46), E6274–83 https://doi.org/10.1073/pnas.1510133112 (2015).
10. Lee, E. *et al.* ACT-PRESTO: Rapid and consistent tissue clearing and labeling method for 3-dimensional (3D) imaging. *Sci. Rep.***6** (1863), https://doi.org/10.1038/srep18631 (2016).
11. Li, Y., Jianyi, X., Peng, W., Tingting, Y. & Dan, Z. Optimization of GFP Fluorescence Preservation by a Modified uDISCO Clearing Protocol. *Frontiers in Neuroanatomy.***12**, 67 (2018).
12. Madisen, L. *et al.* A robust and high-throughput Cre reporting and characterization system for the whole mouse brain. *Nat Neurosci.***13** (1), 133–140 (2010).
13. Menegas, W. *et al.* Dopamine neurons projecting to the posterior striatum form an anatomically distinct subclass. *eLife.***4**, e10032 https://doi.org/10.7554/eLife.10032 (2015).
14. Murray, E. *et al.* Simple, Scalable Proteomic Imaging for High-Dimensional Profiling of Intact Systems. *Cell.***163** (6), 1500–1514 https://doi.org/10.1016/j.cell.2015.11.025 (2015).
15. Pan, C. *et al.* Shrinkage-mediated imaging of entire organs and organisms using uDISCO. *Nature Methods.***13** (10), 859–867 (2016).
16. Piperno, G. & Fuller, M. T. Monoclonal antibodies specific for an acetylated form of alpha-tubulin recognize the antigen in cilia and flagella from a variety of organisms. *The Journal of cell biology.***101** (6), 2085–2094 (1985).
17. Renier, N. *et al.* iDISCO: A Simple, Rapid Method to Immunolabel Large Tissue Samples for Volume Imaging. *Cell.***159** (4), 896–910 (2014).
18. Renier, N. *et al.* Mapping of Brain Activity by Automated Volume Analysis of Immediate Early Genes. *Cell.***165** (7), 1789–1802 https://doi.org/10.1016/j.cell.2016.05.007 (2016).
19. Schultze, O. (1897). Über Herstellung and Conservirung durchsichtigen Embryonen zum Stadium der Skeletbildung. In Verhandlungen der Anatomischen Gesellschaft (Anatomischer Anzeiger), pg.3–5.
20. Steinke, H. & Wolff, W. A modified Spalteholz technique with preservation of the histology. *Annals of Anatomy.***183**, 91–95 (2001).

21. Susaki, E. A. *et al.* Whole-Brain Imaging with Single-Cell Resolution Using Chemical Cocktails and Computational Analysis. *Cell.***157** (3), 726–739 (2014).
22. Susaki, E. A. *et al.* Advanced CUBIC protocols for whole-brain and whole-body clearing and imaging. *Nature Protocols.***10** (11), 1709–1727 (2015).
23. Susaki, E. A. *et al.* (2020). Versatile whole-organ/body staining and imaging based on electrolyte-gel properties of biological tissues. *Nat Commun* 11, 1982 (2020). https://doi.org/10.1038/s41467-020-15906-5
24. Tainaka, K. *et al.* Chemical Landscape for Tissue Clearing Based on Hydrophilic Reagents. *Cell Reports.***24** (8), 2196–2210 (2018).
25. Watabe-Uchida, Zhu, Ogawa, Vamanrao, U. Whole-brain mapping of direct inputs to midbrain dopamine neurons. *Neuron.***74** (5), 858–873 (2012).
26. Yao, S., Bergan, J., Lanjuin, A. & Dulac, C. Oxytocin signaling in the medial amygdala is required for sex discrimination of social cues. *eLife.***6**, e31373 https://doi.org/10.7554/eLife.31373 (2017).
27. Yun, D. H. *et al.* (2019). Ultrafast immunostaining of organ-scale tissues for scalable proteomic phenotyping. bioRxiv. doi: https://doi.org/10.1101/660373

Figures

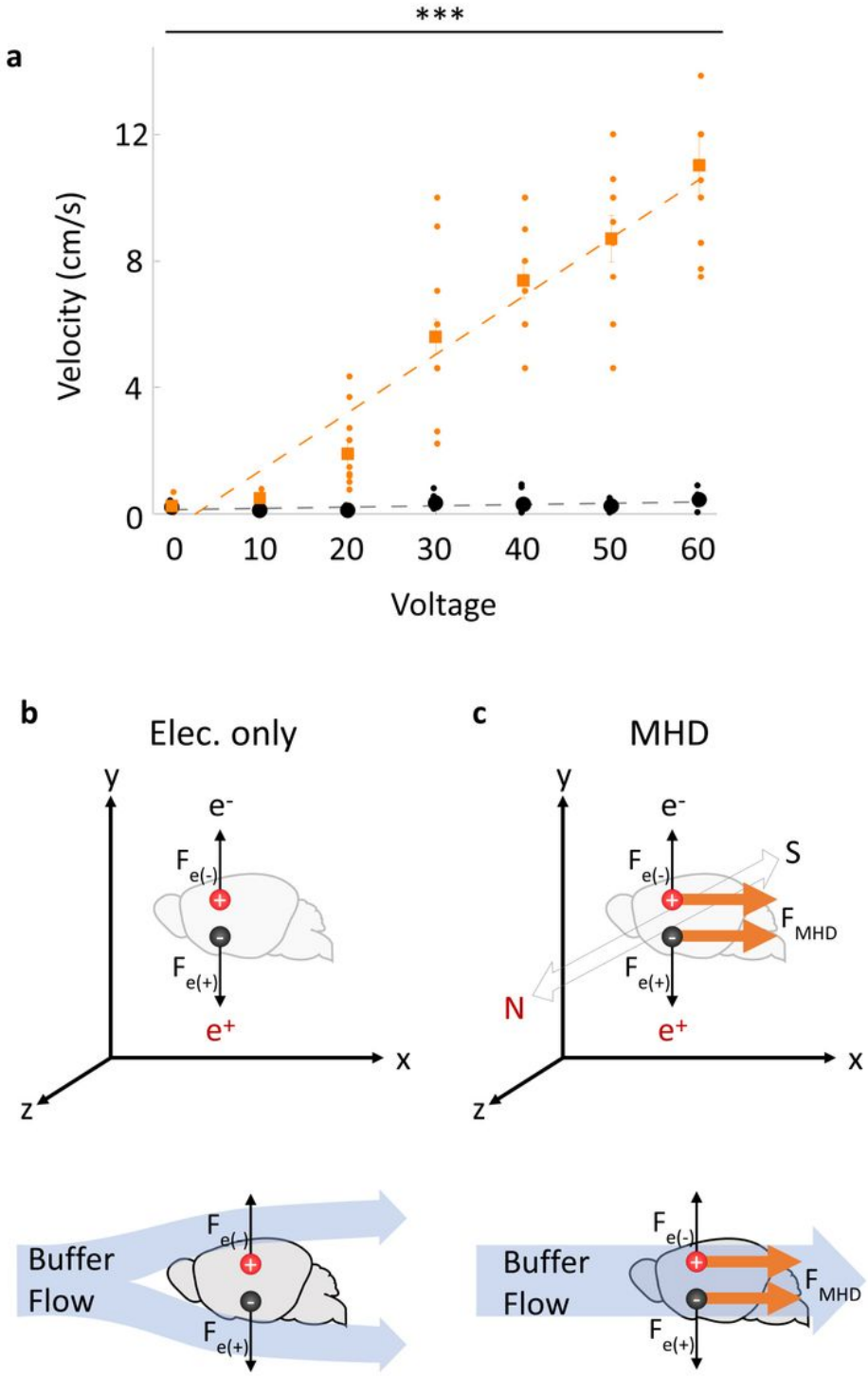

Figure 1

Comparison of voltage effects on buffer velocity between MHD and electrical forces. A) Velocity of sodium alginate spheres through the MHD-accelerated clearing device with (orange) and without a magnetic field (black; N = 7). Error bars show the standard error of the mean of the velocity of the sodium alginate spheres. The MHD condition shows statistically significant increases over the electrical values across all voltages when compared using a 2-way ANOVA ($F(2,6) = 38.51$, $p < 0.0001$). Paired samples T-

test corrected for multiple comparisons at each non-zero voltage also showed significance to α = 0.05 (10V: p = 0.002, 20V: p = 0.0005 , 30V: p < 0.0001 , 40V: p < 0.0001, 50V: p < 0.0001 , 60V: p < 0.0001) . An asterisk indicates significance to α = 0.05. Additional asterisks indicate significance to α = 0.005 (**) or α = 0.0005 (***). The MHD and electric datasets are fit to linear models y=0.1841x−0.4786 (orange) and y=0.004002x+0.1474 (grey) respectively. In B) and C) cartoons illustrate the effects of an electric field B) or conjugated electric and magnetic field C) on positively charged (red) or negatively charged (black) particles. The force induced on each particle by the electric field alone (black arrow) and MHD force (orange arrow) are shown as vectors. The cartoons below show the buffer flow induced by an external pump in conjunction with electrical force B) or by MHD force alone C). The flow of the buffer is shown as blue arrows where the MHD force (orange vector) continues to push buffer through the tissue, while the external pump produces flow around the tissue.

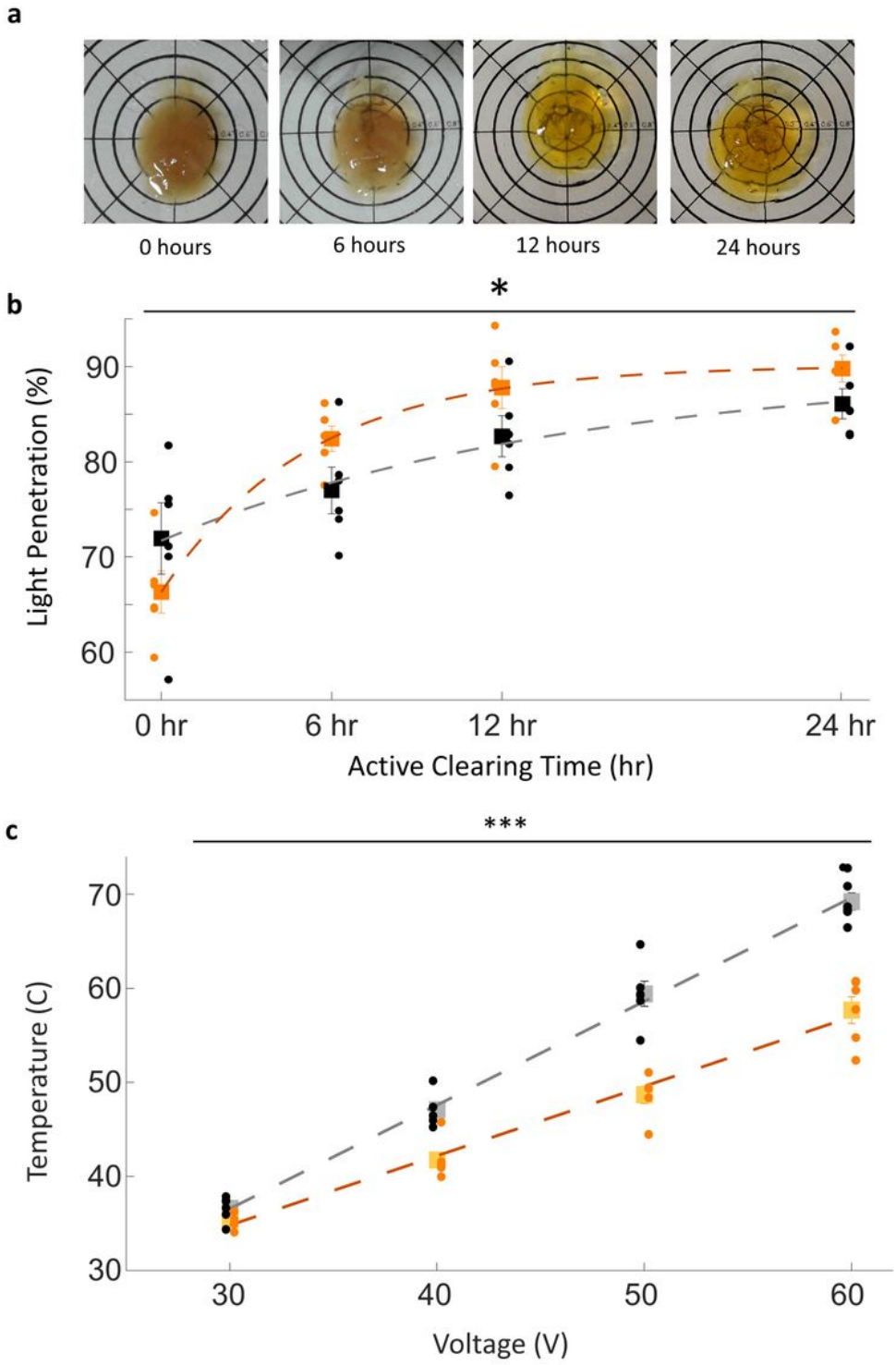

Figure 2

MHD-accelerated clearing of the intact mouse brain. A) Representative examples of intact cleared brains actively cleared with MHD for 0,6,12, and 24 hours and then equilibrated in RI-matching solution (N = 6). B) Measurements of the optical transparency of mouse brains cleared using MHD force (red) or electrical force combined with a pump to circulate buffer solution (black). Transparency was measured as percentage wide-spectrum light penetration through the tissue. Modest statistical significance of an

interaction between electrical and MHD clearing over time is denoted by an asterisk $F(2,3) = 3.24$, $p = 0.0319$. No statistically significant difference was found for the clearing methods alone $F(2,1) = 2.19$, $p = 0.147$. C) Average peak temperature of tissue actively cleared with MHD (orange) or electric-only (black) at voltages ranging from 30 to 60V. Statistical significance over the temperature range as determined by a two-way ANOVA $F(1,3) = 119$, $p < 0.0001$.

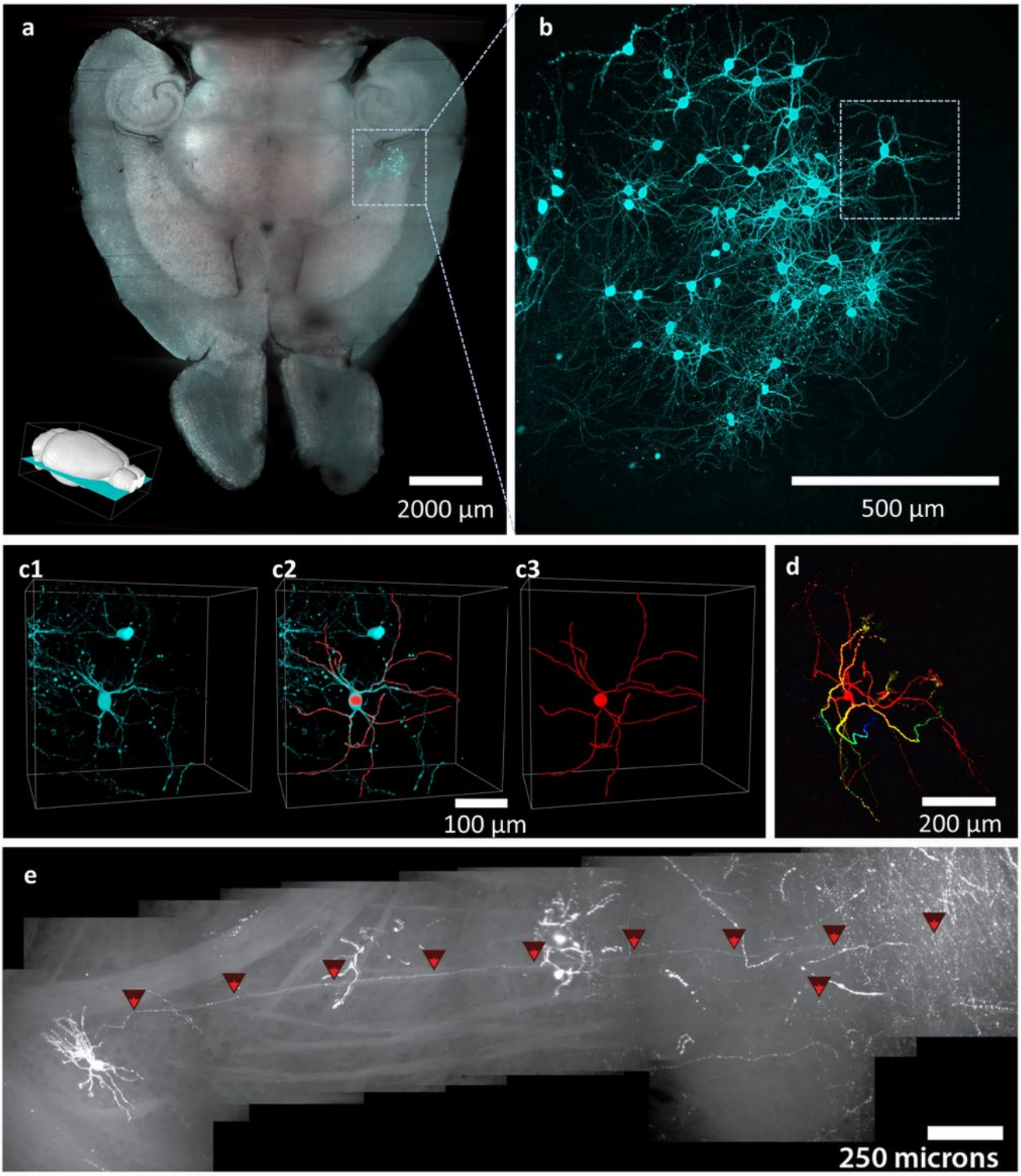

Figure 3

Light sheet microscopy with MHD-cleared tissue. A) Optical slice of an intact mouse brain, which was cleared using MHD-accelerated clearing in the horizontal orientation. The image in the lower left corner shows the positioning of the view in the intact tissue. Tissue was imaged using a Zeiss Z1 lightsheet microscope. GFP-labeled cells are clear in the medial amygdala (cyan). B) A higher magnification image of the infection site corresponding to the location of the dashed box in the horizontal view from A). The image shows that individual cells and associated neural processes are visible deep within the tissue. C) A further zoom of the image in B) located in the dashed box. This image shows an isolated rabies cell (Left), a trace of the cell and its individual neural processes (Right) and an overlay of the cell and the trace (Center). D) Shows a single cell inside the brain and its processes labeled with eGFP and imaged across a 100 μm optical slice. The depth of each process is coded from red (closest to the surface) to blue (deepest) using the imageJ ‘hypercolor’ function. E) Demonstrates that a single axon can be traced through several millimeters of brain tissue into the center of the brain in MHD-accelerated cleared tissue. The cells shown in D) and E) are not from the same sample as in A) through C).

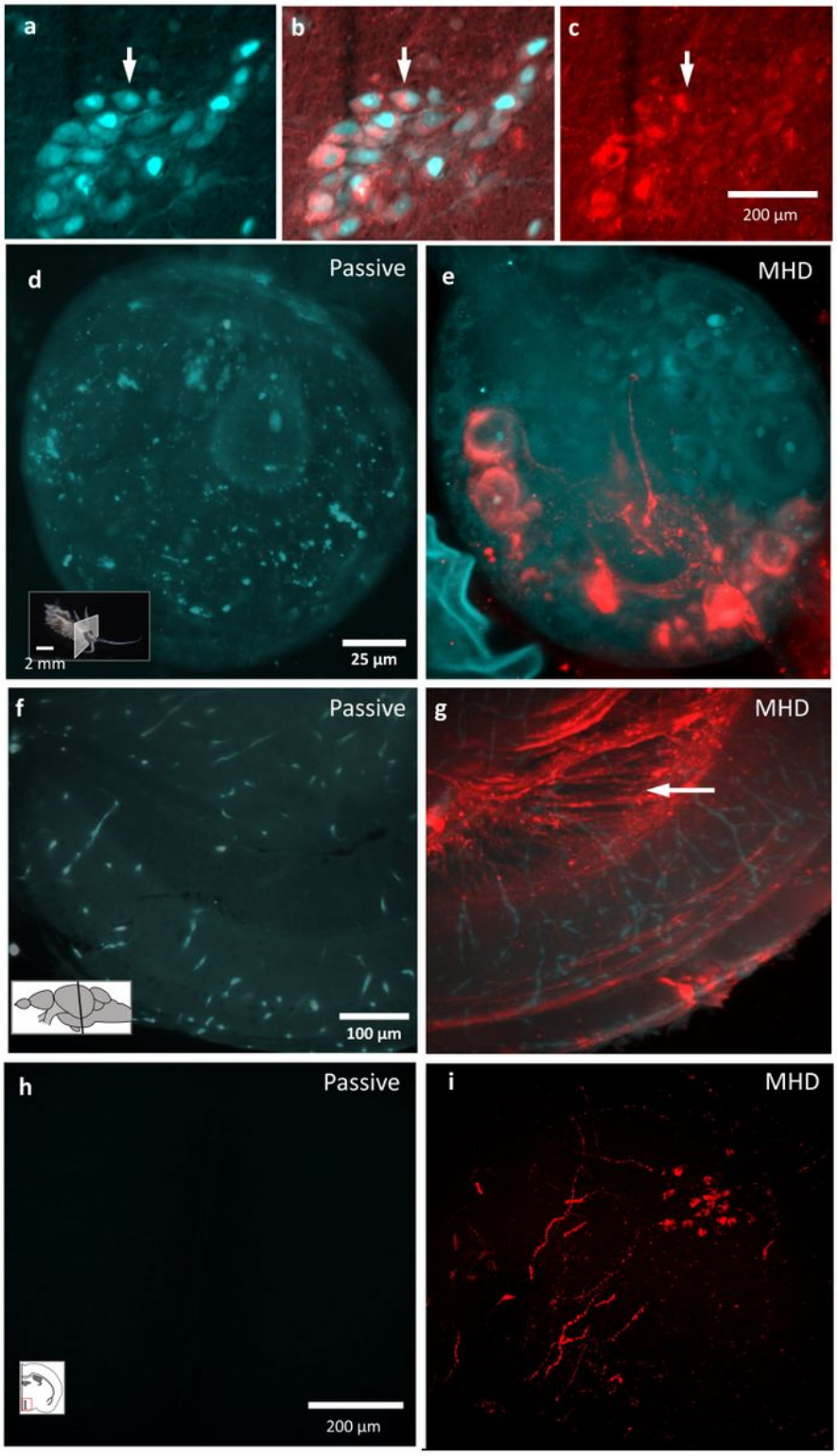

Figure 4

MHD-accelerated antibody labeling of brain tissue from sea slug, zebrafish, and mouse. A), B) High magnification (20x) image of an intact Berghia stephanieae pedal ganglion after MHD-accelerated (B) and passive (A) α-serotonin antibody labeling (red) with tissue autofluorescence (cyan). C, D) Images of a cleared adult zebrafish brain (3mm x 3mm x 6mm) after α-acetylated tubulin antibody labeling (red) with tissue autofluorescence (cyan; Passive labeling: C; MHD-accelerated labeling: D). E, F) Images of cleared

mouse brain sample (6mm x 6mm x 6mm) after α-oxytocin labeling (red) with tissue autofluorescence (cyan; Passive labeling: E; MHD-accelerated labeling: F). G,H,I) MHD-accelerated labeling of adult mouse brain sample (6mm x 6mm x 6mm) after α-vasopressin antibody labeling (cyan) with genetically encoded tdTomato in vasopressin-expressing neurons (red; AVP-cre X rosa26-lsl-tdTomato). Insets indicate the imaging plane.

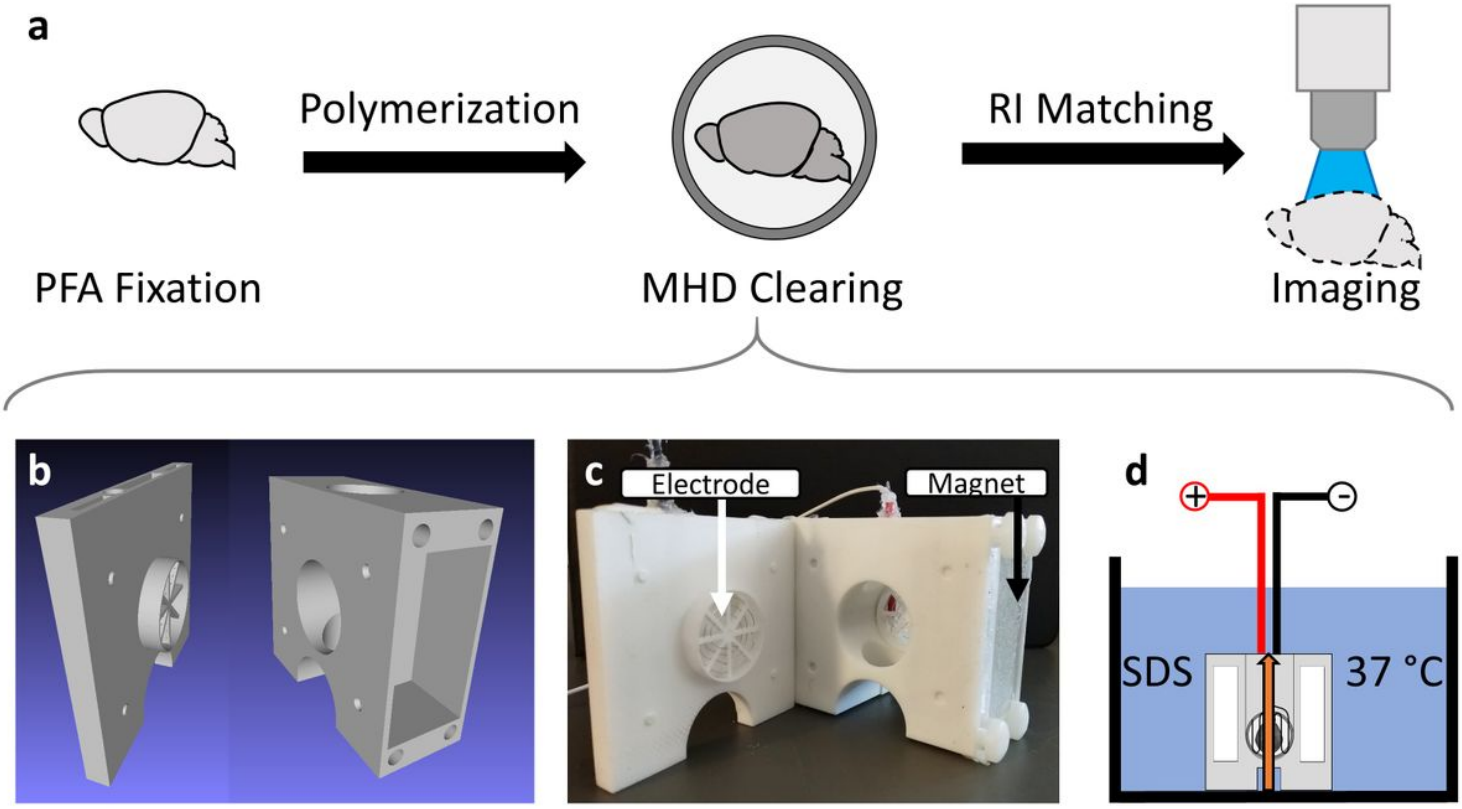

Figure 5

Overview of MHD-accelerated clearing approach. A) Steps required to effectively clear tissue of lipids. B) CAD diagram showing the MHD-assisted clearing device. C) A photograph of the clearing device with tissue chamber exposed and arrows to show the location of the magnets and electrodes in the device. D) A cartoon showing the setup of the clearing device submerged in a container filled with detergent solution held at 37 °C. Tissue was placed in the central chamber where MHD force (orange arrow) produced from the electrical and magnetic fields simultaneously circulate the buffer solution and accelerate clearing.

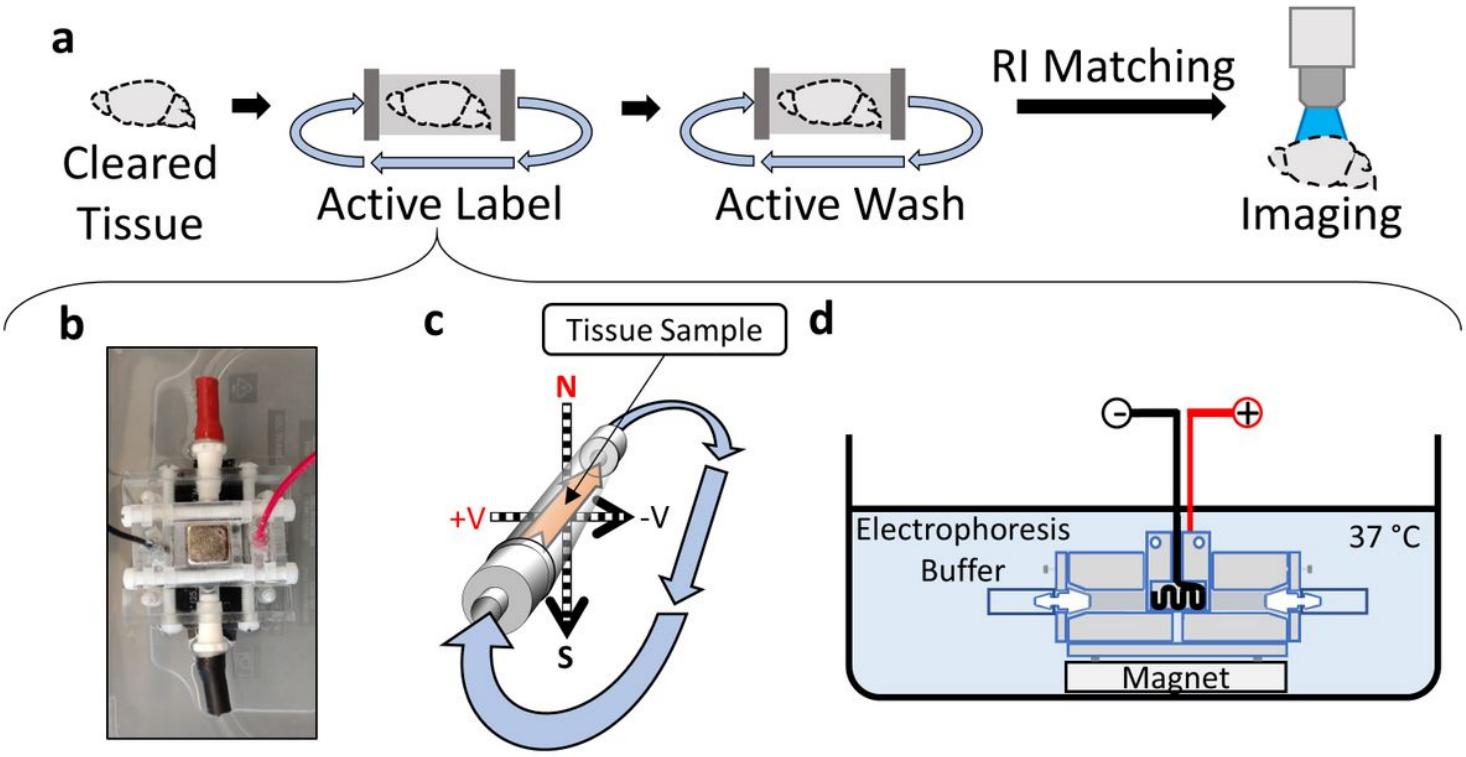

Figure 6

Overview of MHD-accelerated antibody labeling. A) Illustration of the steps required to label and image tissue. B) Picture of the MHD-assisted labeling device. C) Schematic showing the tissue location inside the MHD-assisted labeling device. The direction of the MHD force is indicated by the orange arrow inside the dialysis tubing. The resulting direction of flow of the solution through the closed loop is indicated by the blue arrows. D) Diagram of the antibody labeling device setup for a label. The device is submerged in a bath of electrophoresis buffer held at 37 °C.

Supplementary Files

This is a list of supplementary files associated with this preprint. Click to download.

- Video1.avi
- Video2.avi
- SupplementalInformationV3.pdf
- FigureS1.tif
- FigureS2.tif